NUCLEAR INSTRUMENTS AND METHODS 140 (1977) 413–427; © NORTH-HOLLAND PUBLISHING CO.

TRANSITION RADIATORS FOR ELECTRON IDENTIFICATION AT THE CERN ISR

J. COBB*, C. W. FABJAN†, S. IWATA*, C. KOURKOUMELIS+, A. J. LANKFORD+, G.-C. MONETI++, A. NAPPI†, R. PALMER*, P. REHAK+, W. STRUCZINSKI† and W. WILLIS†

BNL–CERN–Syracuse Univ.–Yale Collaboration

Received 30 August 1976

We describe transition radiators constructed from thin foils of lithium, used to separate electrons from heavier charged particles at the CERN Intersecting Storage Rings (ISR). The optimization of the system of the radiator and detector is discussed, leading to the choice of parameters for this design. The special features of the construction of a structure of lithium is described. Results of a number of different measurements of the transition radiation are given.

1. Introduction

The identification of the mass of energetic particles is one of the most difficult problems in experimental particle physics. It is particularly challenging in the case of identification of the particles at storage rings, where a large solid angle in the centre-of-mass implies covering the same solid angle in the laboratory, and where the use of the most familiar techniques, such as Cherenkov counters, tends to lead to detectors of unreasonably large size. At proton storage rings, such as the CERN Intersecting Storage Rings (ISR), the large size of the source region is a further constraint on the design of large solid angle experiments as a compact detector size is only possible if the angular acceptance is large for the particles to be identified. This is another consideration which makes the use of focusing Cherenkov counters particularly difficult.

Our experiment required us to identify electrons in the energy region of a few GeV, while rejecting hadrons. We wished therefore to reject particles with a Lorentz factor $\gamma = (1-\beta^2)^{-\frac{1}{2}}$ less than 100, while accepting particles with γ higher than about 1000. Since this threshold refers to particle velocities different from c by less than one part in 10^{-4}, methods that depend on direct measurement of particle velocity may be ruled out. The detectors which give a response that depends upon γ, all take advantage of the fact that the electric field of a relativistic particle becomes concentrated in the plane perpendicular to its motion, by the Lorentz transformation. The field measured in the laboratory in that plane increases proportional to γ. A number of aspects of the interactions of charged particles with matter are influenced by this concentration of the field.

* Brookhaven National Laboratory, Upton, NY, U.S.A.
† CERN, Geneva, Switzerland.
+ Yale University, New Haven, Conn., U.S.A.
++ Syracuse University, Syracuse, N.Y., U.S.A.

As γ increases, different absorption processes can take place at greater distances from the trajectory of the particle, and the mechanisms of energy loss become more effective. However the polarization of the atoms of the interacting medium arrests this spreading of the field, leading to a saturation of the increased energy loss at some value of γ. The Cherenkov radiation is one of the manifestations of this polarization, and it too saturates at rather low values of γ, for material of normal density. These saturation effects, and the Cherenkov threshold, can be displaced to high values of γ by using material of very low density, but the small amount of such energy loss then leads to a necessity for very long absorbers which are hardly possible in a large solid angle detector.

The phenomenon of transition radiation (TR) offers a solution to this problem. This process was predicted by Ginsburg and Frank[1]). Its properties in the X-ray region were pointed out by Garibian[2]), who pointed out its possible application in high-energy physics[3]).

Transition radiation is produced when a charged particle traverses an inhomogeneous medium. In the portions of the medium which have a low density, the polarization effects are small and the field has a relatively great extension in the transverse plane. When the particle traverses an interface into the denser portion of the medium, the field in the transverse plane is reduced by polarization. Associated with this redistribution of charge in the medium is a radiation field, which propagates far from its origin. In this process are combined the high transverse electric field of a relativistic particle in vacuum, and the relatively large energy loss made possible by the denser medium. The frequency of the radiation observed is related to the Fourier transform of the field of the particle and thereby to its γ. By selecting the frequency of the

radiation, an effective threshold is built into the detector. In this way it is easy to create a threshold high enough so that the unwanted particles cannot be detected. The problem rather is to attain a sufficient efficiency for the wanted particles, because the number of photons radiated per interface is of the order of 1/137. This has been the difficulty which prevented the adoption of this technique in high-energy physics experiments, although there have been many investigations of the phenomenon[4]).

In this paper we describe a transition radiator which has been carefully optimized and constructed with the exotic material of thin lithium foil[5]). This radiator, with its associated X-ray detector described in a companion paper[6]), is the first transition radiation detector which allows both useful rejection of hadrons and a good efficiency for the detection of electrons of a few GeV, with a *single* radiator. The detectors which have been tested previously required, at least in this energy range, a number of successive radiators and X-ray detectors to achieve this performance. Such an arrangement requires so much length that it is not attractive in a large solid angle set-up.

The theory of this effect has been described in a number of recent review articles[2, 7]), and we will sketch here only enough to enable the reader to understand our results.

A particle crossing a single interface of two semi-infinite media emits TR-photons in the X-ray range with a spectral density

$$\frac{\mathrm{d}W}{h\,\mathrm{d}\omega\mathrm{d}\Omega} = \frac{\alpha}{\pi^2}\left|\frac{\theta}{\eta_1} - \frac{\theta}{\eta_2}\right|^2 = \frac{\alpha}{\pi^2}\,|a(\omega)|^2\,, \tag{1}$$

where $\eta_i = \gamma^{-2} + \theta^2 + \xi_i^2$, and $\xi_i = \omega_{\mathrm{plasma},i}/\omega$ is the ratio of the plasma frequency in medium i to the frequency ω of the emitted photon and θ is the angle of emission with respect to the particle trajectory. If the particle traverses a single foil of thickness d_1, the emitted spectral density is

$$\frac{\mathrm{d}W^{(1)}}{h\,\mathrm{d}\omega\mathrm{d}\Omega} = \frac{\alpha}{\pi^2}\,|a(\omega)|^2\,4\sin^2\tfrac{1}{2}\phi_1\,, \tag{2}$$

where we assume the frequency of the photon is large compared to the ionization potential of the atoms in the medium, and we ignore the absorption of the wave as it traverses a single foil. The phase angle is defined as

$$\phi_i = \frac{\omega d_i}{2c}\,\eta_i\,.$$

The generalization of eq. (2) to N foils of thickness d_1, spaced periodically d_2 cm apart, is given by

$$\frac{\mathrm{d}W^{(N)}}{h\,\mathrm{d}\omega\mathrm{d}\Omega} = \frac{\alpha}{\pi^2}\,|a(\omega)|^2\,4\sin^2\tfrac{1}{2}\phi_1\,F_N^{\mathrm{coh}}(\phi_1+\phi_2)\,, \tag{3}$$

where

$$F_N^{\mathrm{coh}}(\phi) = [1 + \exp(-N\sigma) - 2\exp(-N\sigma/2)\cos N\phi]/$$
$$/[1+\exp(-\sigma) - 2\exp(-\tfrac{1}{2}\sigma)\cos\phi]\,,$$
$$\sigma = \mu_1 d_1 + \mu_2 d_2\,,$$

and μ_1 and μ_2 are the linear absorption coefficients for the emitted radiation in the two media. The angular distribution of the radiation consists of a Bragg-like pattern and contains no information about the particle. Therefore one loses little information by integrating over the angle. Eq. (3) can be integrated approximately, giving

$$\frac{\mathrm{d}W^{(N)}}{\hbar\,\mathrm{d}\omega} = \frac{4\alpha}{\sigma(\kappa+1)}\,[1-\exp(-N\sigma)]\times$$
$$\times\sum_n \theta_n\left(\frac{1}{\rho_1+\theta_n} - \frac{1}{\rho_2+\theta_n}\right)^2[1-\cos(\rho_1+\theta_n)]\,, \tag{4}$$

where

$$\rho_i = \frac{\omega d_1}{2c}\,(\gamma^{-2}+\zeta_i^2)\,, \qquad \kappa = d_2/d_1\,,$$

$$\theta_n = \frac{2\pi n - (\rho_1 - n\rho_2)}{1+n} > 0\,.$$

We have checked that for all the radiators we discuss in this paper, a numerical integration gives the same results as this approximation.

It is clear from an inspection of these formulae that the design of transition radiators is dominated by the consideration of interference effects. This is most trivially evident when one notices that these formulae explicitly show that the radiation goes to zero as the foil thickness is reduced to zero or the gap between foils vanishes. This effect is usually expressed in a different way by saying that the transient field exists over a certain region known as the formation zone. However, the formulae show the interference effects to be important even when the distances are larger than those corresponding to the formation zone. Doubt has often been expressed in the literature as to whether the radiation is really coherent over these longer distances. Two of the authors of the present paper have undertaken an investigation where quantitative measure-

ments were made with radiators which were designed to maximize the interference effects[8]). The results establish very clearly that the radiation is coherent not only between the two surfaces of a single foil separated by distances much greater than the formation zone, but also the radiation between two different foils is coherent for substantial distances. These measurements confirmed not only the spectral distribution of the radiation, but demonstrated that the absolute magnitude of the radiation was correctly given by the theory within 5% or 10%. Thus we are confident that we can use our calculations based on the above formulae to design an optimum detector–radiator system, as outlined in the next section.

2. Design of an optimum detector

We find that it is important to be cognizant of each of the many parameters which could possibly be varied in the overall transition radiator–detector system. This is particularly important because of the small number of transition radiation photons per foil.

Our optimization studies were actually carried out using computations directly from the formulas of section 1, but the qualitative considerations involved can be concisely described using variables introduced by Artru et al.[7]). They noted that any transition radiator can be described in terms of a universal function of certain dimensionless parameters, independent of the particular material used or the spectral range involved. These parameters are:

a dimensionless particle energy,

$$\Gamma = \gamma/\gamma_1 , \tag{5}$$

where

$$\gamma_1 = \tfrac{1}{2} d_1 \, \omega_{\text{plasma},1} ;$$

a dimensionless frequency

$$\nu = \omega/\gamma_1 \cdot \omega_{\text{plasma},1} , \tag{6}$$

and the ratio $d_2/d_1 = \kappa$, and $c = 1$. In convenient units $\gamma_1 = 2.5\,(\omega_{\text{plasma},1}/\text{eV}) \times (d_1/\mu\text{m})$. It is most instructive to study the universal curves given in ref. 7. Certain qualitative features are important for our purpose:

1) Very little radiation is produced for $\nu > 1$, for any Γ.
2) There is a strong peak at $\nu = 0.3$ for $\Gamma > \frac{1}{2}$.
3) There is a strong interference minimum at $\nu = 0.18$, due to a phase slip of π within the foil. There are further peaks of radiation for lower values of ν, but in practical radiators these are absorbed. The net result is that most of the radiation comes out in a relatively narrow frequency band for $\nu \cong 0.3$.
4) The amount of radiation is small for $\Gamma < \frac{1}{2}$. It increases rapidly for values of γ as large as 2, and beyond that increases only logarithmically if κ is very large and the gaps are in a vacuum. For finite κ or with a gas in the gaps, the radiation approaches an asymptotic value for a certain value of Γ, usually less than 10.
5) d_2 can be made such that the phase slip in the gap is 2π and there is constructive interference between foils. The required value of d_2 is a function of Γ. For an optimized detector this should happen in the region of $\Gamma = 1$. As confirmed by our numerical studies, a radiator designed to have the optimum performance to give a good efficiency near its threshold will have $\Gamma = 1$, $\nu = 0.3$, $\kappa \cong 5$. Given a material with a certain ω_{plasma}, the foil thickness is determined by the desired threshold $\gamma = \gamma_1$, using eq. (5).

It remains to choose the material and structure for the radiator, and to design the X-ray detector. We have in mind detectors where the radiator consists of many foils, followed by a single X-ray detector. Since there is no magnetic field, and the angle of the transition radiation is very small, the X-ray detector will also see the ionization due to the charged particle. Only the transition radiation which escapes from the

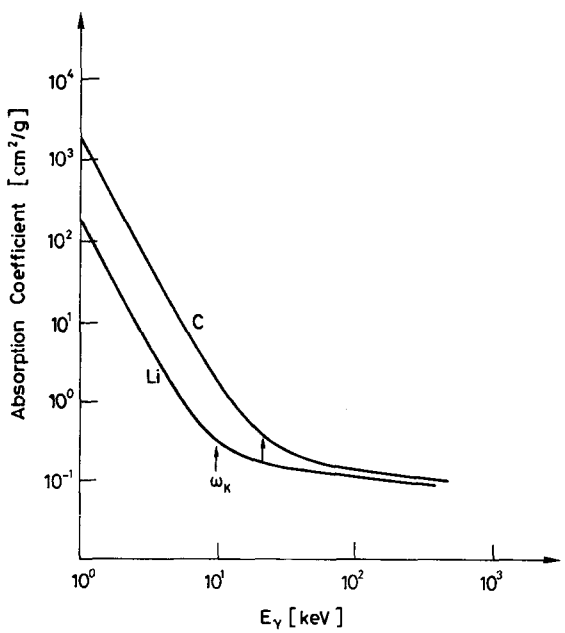

Fig. 1. Absorption cross-section for X-rays as a function of energy for two different materials.

stack of foils is useful. Therefore the absorption of the material used in the stack for the frequency corresponding to $v = 0.3$ is crucial. The detector of the radiation can be characterized by the amount of material necessary to absorb the X-rays and the energy deposited from the ionization of the charged particle in that amount of material. Thus the radiator must have the *lowest* absorption possible, and the detector must have the highest.

The dependence of the X-ray absorption on energy and the Z of the absorber is shown in fig. 1. In the energy range of interest, the absorption is dominated by the photoelectric effect. The absorption cross-section σ varies with the energy of the photon as $E^{-3.5}$ and with the atomic number of the absorber as $Z^{3.5}$, for the portions of the curve between absorption edges. For photon energies above a certain value ω_k, the dominant process becomes inelastic scattering with a flat energy dependence. For electron detection, we usually wish to make γ_1 the threshold value, as low as possible. This forces us to choose a low operating frequency. However, if the photon energy is chosen on the sharply rising part of the absorption cross-section of the radiator material, the resulting absorption will strongly limit the effective number of foils. Thus one can see, and numerical studies confirm, that the best value of the operating X-ray energy for a given material is a value near ω_k. Then one finds that ω_k is proportional to Z, and the absorption length at ω_k is rougly constant, when measured in g/cm^2.

The optimum thickness for the *detector* is approximately one absorption length for X-rays with an energy of $2\omega_k$, where ω_k is determined by the *radiator*. From many points of view the most suitable detector for these X-rays is a proportional chamber. The proportional chamber gas which gives the best ratio of absorption length to energy deposited by a charged track, is xenon gas, for X-ray energies above the absorption edge at 5 keV. The absorption length, and therefore the energy deposited in the detector from ionization on the charged track, varies as $\omega_k^{3.5}$ between 5 and 35 keV:

$$\text{Ionization} \propto \omega_k^{3.5} \propto (Z_{\text{radiator}})^{3.5}. \tag{7}$$

The other factor which enters the optimization is the plasma frequency of the radiator, which is proportional to the square root of the density. This does not have a dependence which can be given analytically, though of course it has a tendency to increase with Z.

Fixing the mean energy of the detected X-ray at $\bar{\omega} = \omega_k$, and for $v = \frac{1}{3}$, we obtain from eq. (6) the corresponding value of the lowest natural threshold as

$$\gamma_1 \geq \gamma_0 = 3\omega_k/\omega_{\text{plasma}}. \tag{8}$$

Table 1 gives values of this threshold for a number of materials. The optimum thickness of the radiator foil is then given by

$$d_1 = 6\frac{\omega_k}{\omega_{\text{plasma}}^2}.$$

TABLE 1

Relevant properties of possible radiator materials.

Material	Density, ρ	ω_p	ω_k	Natural threshold	Relative $\frac{\text{signal}}{\text{ionization}} = \frac{S}{I}$	Relative number of photons
	(g/cm^3)	(eV)	(keV)	γ_1	$= \left(\frac{\omega_{k,\text{LI}}}{\omega_k}\right)^{3.5}$	$= \left(\frac{\rho}{\rho_{\text{LI}}}\right)^{1.25} \times \frac{S}{I}$
H_2	0.07	7.86	2.8	1070	77	6.3
LiH	0.82	19.1	8.9	1400	1.35	2.4
Be	1.85	26.9	13.6	1520	0.30	1.45
Li	0.53	14.2	9.7	2050	1.00	1.00
B	2.37	31.1	17	1640	0.14	0.92
C (diamond)	3.52	39.4	21	1600	0.067	0.71
C (graphite fibres)	2.25	31.5	21	2000	0.067	0.41
B_4C	2.52	32.3	19	1760	0.095	0.67
Al_2O_3	3.97	41.0	45	3300	0.0047	0.058
Al_2O_3 for photons below K-edge at:	1.5			110	0.05	0.62
CH_2	0.9	18.6	19.3	2900	0.09	0.18

The absorption of photons of energy ω_k in one foil of density ρ is

$$\sigma d_1 \rho = 6\sigma\omega_k \frac{\rho}{\omega^2_{\text{plasma}}} \propto \sigma\omega \propto Z,$$

since $\omega^2_{\text{plasma}} \propto \rho$.

If there are a large number of foils, the radiation at the exit comes from an effective number of foils:

$$N_{\text{eff}} = \frac{1}{1-e^{-\sigma d_1}} \simeq \frac{1}{\sigma d_1} \propto \frac{1}{Z}. \tag{9}$$

The number of photons emitted per foil integrating over the peak near $v = \frac{1}{3}$, is independent of the parameters and is approximately 1/100. The total number of photons emerging from the radiator then is

$$n_\gamma \propto 1/Z.$$

Notice that this is independent of the density of the material but strongly dependent upon Z. The total energy radiated is

$$E_{\text{tot}} = \omega_k\, n_\gamma \simeq \text{constant}, \tag{10}$$

independent of Z and of the density.

The ratio of the transition radiation signal in the detector to the ionization loss of the charged particle is, combining eqs. (7) and (10),

$$\frac{E_{\text{total}}}{\text{Ionization}} \propto \frac{1}{Z^{3.5}}.$$

Thus the signal to background ratio is an extremely strong function of Z. Moreover, since there are at best only a few photons to be detected, the number of photons increases as Z^{-1}, so that the statistical fluctuations decrease as well, leading to a shrinkage of the width of the transition radiation peak proportional to $Z^{-\frac{1}{2}}$. The net result is that even a small change in Z produces a drastic effect on the performance of the radiator and detector system. Most previous radiators have been constructed of foils which are similar to CH_2, which is shown in table 1 to be about an order of magnitude worse than lithium. This difficulty can be evaded only by the use of multiple radiator detector layers and a suitable processing of the signals, a very cumbersome system. On the other hand, with the lithium radiator a sufficient number of photons are obtained to provide efficient detection in a single radiator detector assembly. Furthermore, the ratio of transition radiation energy to charged particle ionization is sufficiently large to provide a good rejection of the tail of the ionization spectrum.

It may be interesting to see how these considerations are affected if we insist that the threshold should be lower than the natural threshold value. Let the threshold be given by

$$\gamma_1 = R\gamma_0, \qquad R < 1.$$

In this case the foil thickness is proportional to R, and the peak value of the photon energy distribution is

$$\bar{\omega} = R\omega_k,$$

so that the photon absorption cross-section per electron in the absorber is increasing as $R^{3.5}$, and the absorption per foil is

$$\sigma d_1 \rho \propto R/R^{3.5} = 1/R^{2.5},$$

so that the effective number of foils or the emerging number of photons varies as

$$n_\gamma \propto R^{2.5},$$

carrying total energy

$$E_{\text{tot}} \propto R^{3.5}.$$

However, the length of absorber necessary to capture these photons has the *same* dependence on R, so that the signal to background ratio is *constant*. The average signal may be misleading when the number of photons becomes less than 1. Usually there is a very small signal corresponding to no transition radiation photon, but when such a photon is detected the signal is relatively large. One way of dealing with this situation is to treat the counter as a Yes–No device. Many layers of radiator and detector are needed in this case to obtain adequate photon statistics. Note that the number of photons produced and emerging from the radiator for a given threshold is still inversely proportional to Z, but also involves the density, as shown in table 1. There will be the same strong advantages using the lowest possible Z as long as the energy of the individual photons is large enough to be handled with the techniques used in the detector.

If it is desired to increase the threshold, there are two methods available. Either $\bar{\omega}$ can be increased, or the density of the material can be artificially lowered in a suitably fine-grained manner. If $\bar{\omega}$ is increased, the number of photons remains the same but the absorption length in the detector goes as $\bar{\omega}^3$, while the signal only increases proportionally to $\bar{\omega}$, a disadvantageous scaling. Therefore it is better to take the second alternative and try to use the same material but with an

artificially reduced density. The considerations on the Z of the radiator remain the same.

3. The choice of the radiator material

If we do not wish to deal with the cryogenic materials, hydrogen and helium[9]), the available materials with very low Z are lithium, lithium hydride, and beryllium. Lithium hydride looks attractive since it has an effective Z lower than the pure metal and a substantially higher density. It could conceivably be cast or pressed into thin sheets, but lithium hydride is a hazardous material, and in such finely divided form it would be very dangerous indeed. A lithium hydride radiator made with rather course grains has been reported in the literature[10]), but the thickness of the grains was so much greater than the optimum value that its performance was not interesting.

Beryllium also has a favourably high density, but it is quite expensive in the form of thin foils, and its handling is made difficult because of its toxic character. In appplications involving small areas, these objections might be overcome and it could well be the material of choice.

On the other hand, we have found that it is possible to make satisfactory radiators from pure lithium metal. It is extremely ductile and can be rolled to thin sheets. It can be formed in such a way that it becomes self-supporting, as described in the next section.

The special properties of lithium metal which require comment are: its extreme softness, its flammability, and its tendency to react with water. The softness is in some ways an advantage when one wishes to roll it with large reduction factors, but the difficulty of making a satisfactory structure using only lithium can be appreciated by noting that the ultimate tensile strength is about one-twentieth that of lead. We have observed that there is no detectable work hardening, and plastic flow results already at elongations $<10^{-3}$. The clean metal has a tendency to stick to itself, but our lithium had a thin layer of oil on the surface*. We did not observe any tendency to creep when the lithium was stressed well below its yield point.

We found that the lithium foils and stacks of foils would burn when ignited with a hot flame, but not explosively. The fumes from the burning metal are hazardous. Special fire extinguishers with an adequately dry powder must be used.

Lithium reacts strongly with water, though not as strongly as the heavier alkali metals. In very dry air it forms a thin oxide layer which protects the metal, just as in the case of aluminium. However, this layer is attacked by water vapour and if the relative humidity of the air is greater than a few percent the foil loses its normal metallic lustre, and is soon converted into a white powder. It is necessary, therefore, to handle it in an environment with a relative humidity of about 2% or less. It is difficult to carry out fabrication on the required scale inside a glove box, and we found it necessary to prepare a small room as a dry laboratory. The surfaces of this room were tightly sealed and entry was by means of a vestibule with double doors, to prevent direct contact with the outside air. Air in the entire room was changed approximately once per minute and put through an air-drying system. The air was cooled by a standard air-conditioning refrigerator and then passed through a commercial lithium chloride air dryer†, which is based on a revolving drum which is continuously regenerated by a hot air stream. The humidity in the laboratory was continuously monitored and was maintained at a dew point of about $-35\,°C$+. The capacity of this system is quite sufficient to maintain the humidity despite the presence of several people working in the laboratory and a good deal of use of the doors to the outside. No health difficulties were experienced by workers spending several hours a day in the laboratory for extended periods.

The dry air ducted into the laboratory was arranged to flow over the work bench before dissipating into the room. Lithium could be left open on this bench for several months without showing apparent surface damage or increased X-ray absorption.

The purity of the lithium and its freedom from adverse effects due to surface films was verified by frequent measurements of the X-ray absorption. A variety of standard X-ray sources was used in conjunction with a thin sodium iodide scintillation counter. We observed a 25% excess X-ray absorption due to the oil film on our foil. This could be removed by cleaning with a solvent, but we preferred to keep the oil for ease of handling. The clean foil showed at most a few percent excess absorption due to oxide and nitride surface layers. These measurements were made on finished foil stacks as well as on samples of the rolls of foil as delivered.

4. Design and fabrication of the radiators

In section 5 it is shown that the optimum parameters for the radiator are those given in table 2. The mechani-

* Foote Mineral Company, Exton, Pennsylvania, U.S.A.

† Cargocaire Engineering Corp., Amesbury, Mass., U.S.A.

+ Manufactured by Siemens AG, model M55-402-12 with read-out unit M740-C9701-T151.

TABLE 2
Geometrical and nuclear parameters of the Li–TR radiators.

Radiator	Base area (cm^2)	Depth (cm)	Number of foils	Thickness of foils (μm)	Radiation length	Nuclear collision length
1	34 × 76	19	650	~53 ± 5	0.022	0.034
2	52 × 126	22	700	~53 ± 5	0.025	0.037

cal problem of the construction is to provide a method of supporting 50 μm lithium foils with a uniform spacing of 300 μm, over a depth of about 700 foils. We needed to construct radiators with a surface area of approximately 600 by 1200 mm^2. The design did not allow for any appreciable frame structure at the edges of the radiators, so it was necessary to find a design for stacks of foils which would be self-supporting. The detectors are used in a large solid angle coverage of a fairly small source, and consequently have the form of a truncated pyramid, as shown in fig. 2. The radiator must be self-supporting against the force of gravity in any direction. Furthermore, to avoid absorption no supporting structure can be placed between the radiator and the proportional chamber, even when the weight of the radiator is forcing it toward the chamber window.

These are difficult conditions when it is realized that the strength of the lithium is very small, about 0.05 kg/mm^2, and that it is not possible to use any appreciable quantity of any other material to support the lithium, because all other materials have much greater X-ray absorption. Aside from the fact that the design allows no frames at the edges, it would not be useful to try to support the foils on frames because the strength of the foils is insufficient to maintain them over the required area when they are in a horizontal plane.

In this case the best method to maintain foil spacing seems to be some arrangement of indentations on the foils which bear on the adjacent foil. If this structure is subject to compressive loads, the method of failure is by bending of the foil between its points of support. If the indentations consist of a nearly random pattern of point indentations, it is easy to compute from the properties of the material that the loading due to the weight of a stack of 700 foils, 1.5 g/cm^2, will crush the structure unless the indentations cover essentially the whole area. This failure is avoided by the structure shown in fig. 3. This arrangement is generated by

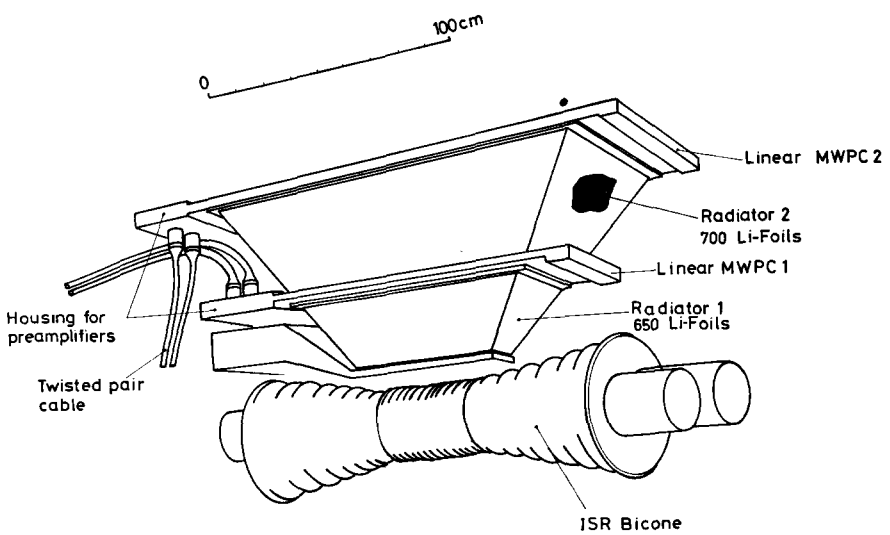

Fig. 2. Artist's impression of one TRD module installed in ISR intersection 8. The two circulating proton beams collide in the cylindrical part of the bicone over a length of about 40 cm. The energy information collected from the 130 wires of the two MWPCs is transmitted over six groups of 60 m long, twisted-pair cable to the experimenter's counting room.

rolling alternate foils in the stack with the longitudinal indentations shown extending along the entire length of the strip of lithium. This structure is relatively strong because the span of the flat portion of lithium between the points at which the loading is applied is small. The observed compressive strength of this structure is about 50 g/cm^2, which can be understood if it is assumed that the points of contact do not slip when subjected to the loading.

The stacks of foils are composed of subassemblies which are generated by a winding procedure, as illustrated in fig. 4. Two foils are wound simultaneously, one of which is flat and the other one which receives the indentations of the form of fig. 3 during the winding process. Lithium foil, 50 μm thick and 50 mm wide, leaves the supply roll and passes through a pair of brass rollers which impart the pattern of fig. 3. These rollers are driven by a servo-motor with a speed controlled by a tension measurement on the output side of the rollers. The foil then goes on to a square winding form with slightly rounded corners. The flat foil follows the same course without the forming rollers. The tension must be controlled accurately because of the small strength of the lithium foil. The size of the square winding form can be adjusted to produce stacks of the desired length. After 50 foils have been wound, the wound portion is cut into four stacks with an electric carving knife. This process effectively welds the foil ends together so that each stack is self-supporting. The stacks are then cut to the desired shape with a fine reciprocating saw, and cemented (slow-curing araldite) to the sides of the box which serves to hold their weight and provide a helium atmosphere when the radiator is in use. This procedure can produce about 15 l of volume of radiator per working day.

The open-backed radiator box is mounted directly on the front of the proportional chamber[6]) with only the chamber window separating the radiator and the gas of the chamber. A small flow of helium gas is maintained through the lithium box. To ensure that this helium gas is dry after passing through the lines which bring it to the box, a plexiglass cylinder filled with crumpled lithium foil is inserted just before the line enters the lithium box. If the gas lines have not been adequately dried before use, a deterioration of the lithium is observed at the entrance end of the plexiglass cylinder.

5. Results

We have made a series of measurements to study different aspects of the performance of the radiators constructed in the manner described above. We shall describe here two series of measurements done in test beams at the CERN Proton Synchrotron (PS). The first series utilized magnetic deflection of the beam and detection of the radiation alone with a semiconductor detector, and the second series involved the use of proportional chambers measuring the radiation together with the incident particle.

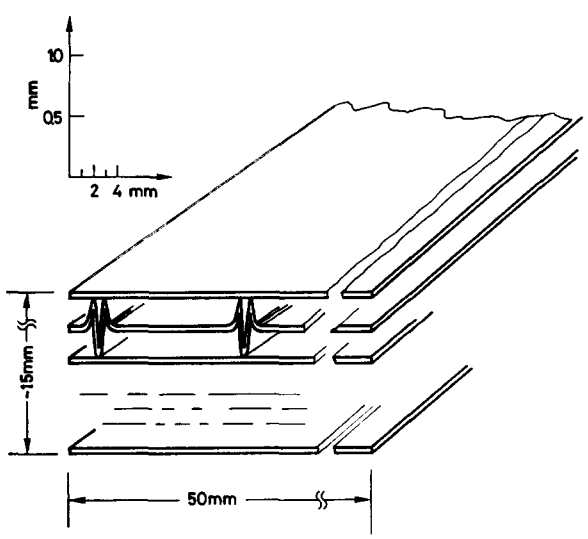

Fig. 3. Cross-section through a Li radiator "brick". The indentations of alternate foils run the full length of the foil.

Fig. 4. Partial view of winding machine. The indented foil passes under a tension roller and is then wound onto a square frame simultaneously with the flat foil.

The first set-up[8]) is shown in fig. 5. The beam is taken from an internal target at the PS at an angle of 4° and swept free of charged particles. A lead plate converts π^0's to give a charged particle beam, dominantly of electrons, which are identified by the gas threshold Cherenkov counter. Hole veto-counters are used to eliminate halo particles. After the electrons traverse the radiator, they are given a small deflection by the second magnet. The transition radiation is detected by a silicon detector, providing an energy resolution of fwhm $\simeq 260$ eV. Measurements were taken at nine different positions of the detector fully covering the spatial distribution of the transition radiation. As the silicon detector has almost 100% detection efficiency over the X-ray frequencies of interest, this measurement gives the energy distribution of the total emitted transition radiation.

Fig. 6. shows the result of such a spatial integration of TR emitted from a 499-foil radiator. This was a simply constructed radiator, with the 50 μm-thick Li foils glued to circular brass frames, of 25 mm inner diameter and 0.2 mm thickness. For comparison, we show for this radiator the calculated yield. Eq. (3) was integrated numerically and Monte Carlo techniques were used to simulate the photon statistics. A small correction was applied for the absorption between the radiator and the silicon detector (two 25 μm-thick polypropylene exit windows of the radiator, two 50 μm-thick mylar windows of the helium bag, 10 cm of air, 556 cm helium at STP). The measured yield of low-

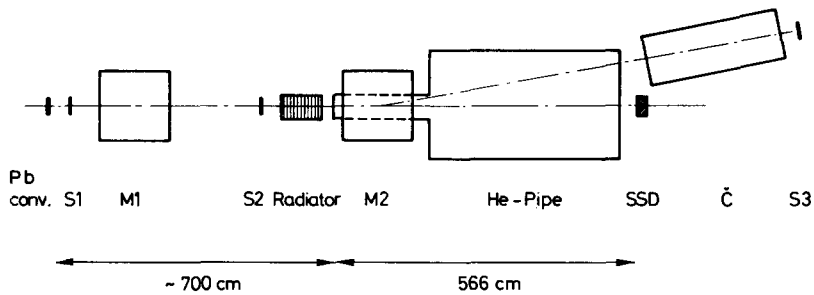

Fig. 5. Experimental layout for the absolute TR-yield measurement using a semiconductor detector. Not to scale.

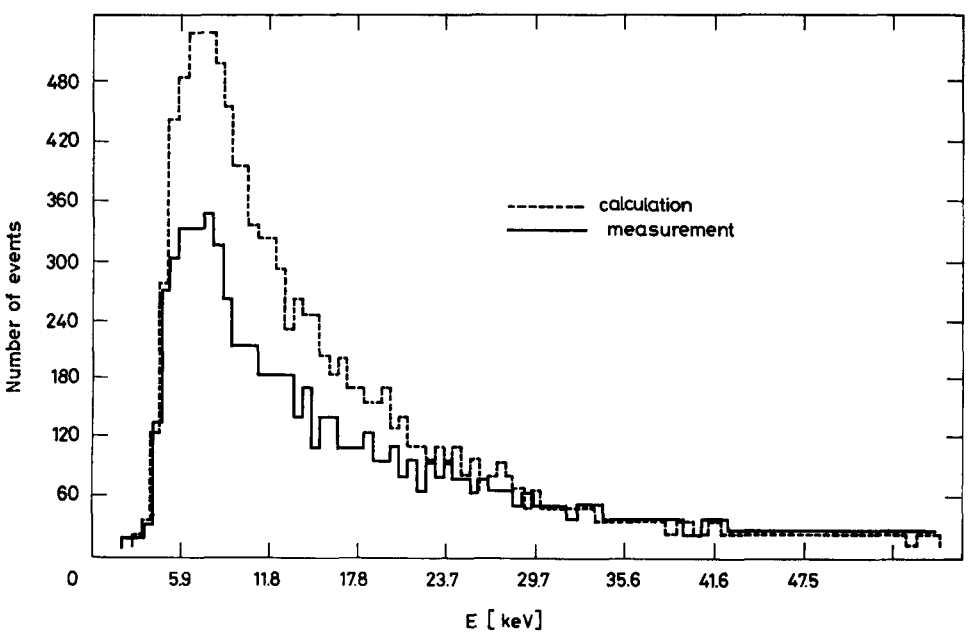

Fig. 6. TR spectrum obtained with the 499-foil radiator; the Li foils had a thickness of 50 μm with a nominal spacing of 200 μm provided by brass frames. The dashed line gives the calculated yield expected for a radiator with perfectly periodic foil spacing; 4000 electrons at $\gamma = 2680$ were recorded.

energy photons is 30% less than expected. Such an effect is expected, if a fraction of the foils are more closely adjacent than the nominal 0.2 mm resulting in a hardening of the emission spectrum. We compute that, on the average, 3.1 TR photons per electron are absorbed in the detector, whereas the measured number is 2.1 photons. The computed average energy absorbed is 36.3 keV, about 20% larger than the measured value of 29.6 keV.

This measured TR spectrum, which reflects the imperfections of a practical radiator, was used to define a frequency-dependent correction factor to give agreement between measurement and calculation for this radiator. In optimization calculations and com-

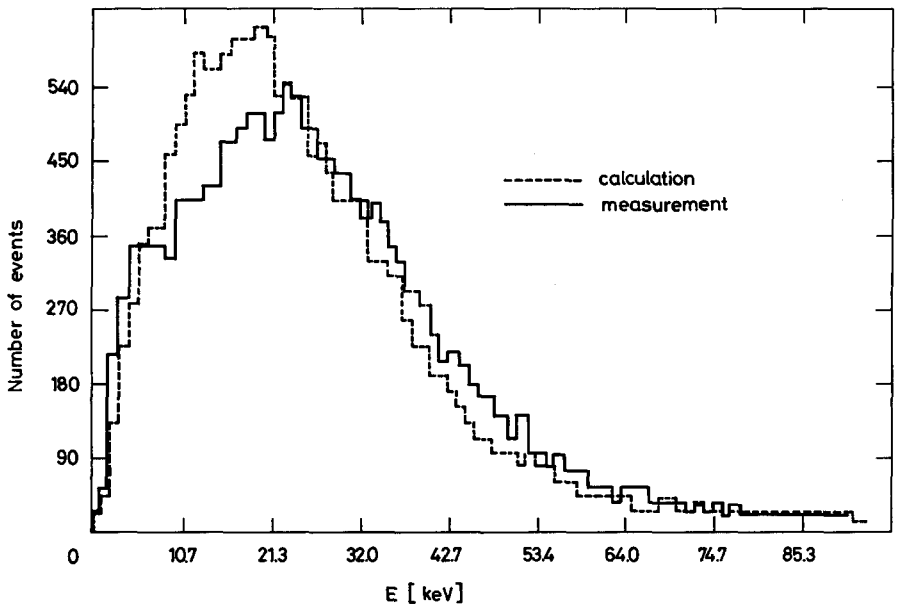

Fig. 7. The TR spectrum obtained from the same radiator as was used in fig. 6 but with the silicon detector replaced by a MWPC. The dashed line is calculated using as input the measured spectrum of fig. 6 and the measured dE/dx loss of the electrons; the response of the MWPC to X-rays was calculated; 17150 electrons with $\gamma = 2680$ were recorded.

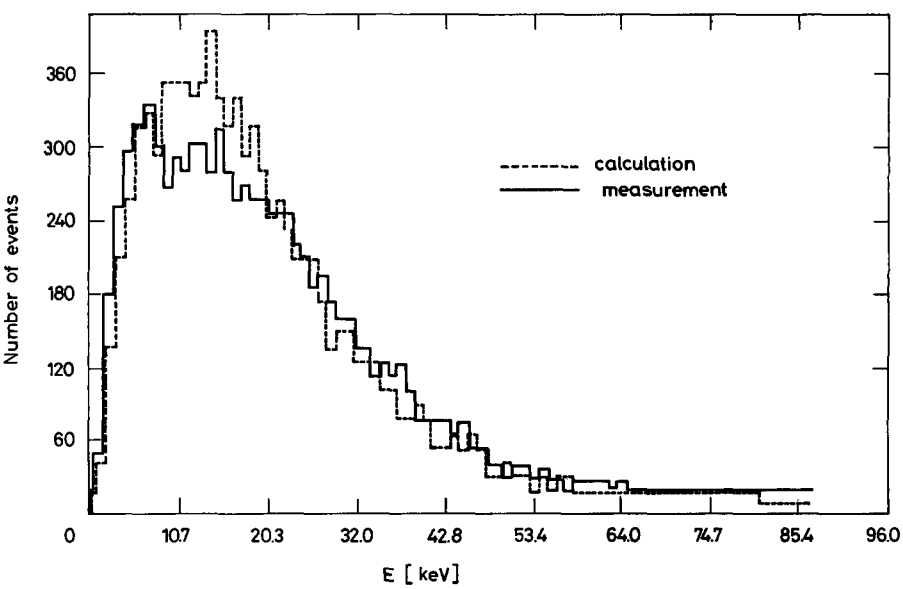

Fig. 8. The TR spectrum obtained with a 350-foil self-supporting radiator (see text), measured with a MWPC; 8650 electrons were recorded at $\gamma = 2680$.

parison of various radiator geometries with calculations, precisely this correction factor was applied as a way to consider and judge radiator imperfections.

A number of stacks were built with different forms of indentations in the foils. We tried forms resembling sine waves and those with smaller and larger distances between the indentations of the form of fig. 3, which was found to give the best yield. The performance of these various radiators was checked in a second series of measurements. The beam layout was similar to that shown in fig. 5. However, the silicon detector was replaced with a small multiwire proportional chamber (MWPC), filled with 80% Xe and 20% CO_2 and placed directly behind the radiator. Therefore, the TR energy was measured superimposed on the ionization loss of the particles.

The previously described 499-foil radiator gives a spectrum in the MWPC, shown in fig. 7. Input for the calculations (unbroken lines) were the 'corrected' single foil yield, the measured dE/dx loss of electrons in the MWPC, and known properties of the gas [absorption cross-section and fluorescent escapes[11]]. The reasonable agreement indicates that the properties of the MWPC are correctly understood. Fig. 8 shows the analogous measurement and calculation for a wound radiator, consisting of 350 foils with indentations as shown in fig. 3, spaced 5 mm apart. The agreement between measurement and calculation implies that this self-supporting radiator gave a TR yield very similar to that of the "frame" radiator. We also tried 6 mm spacing of the indentations, giving somewhat superior results, and therefore this geometry was used for the construction of the final radiators.

Having selected the best form of stack assembly and verified its performance, two large radiators were constructed, which were intended to be used in sequence as one electron identifier at the ISR, as shown in fig. 2. Relevant parameters are given in table 2.

The optimum number of foils for each radiator was estimated through calculations as described previously. The results obtained for the larger radiators are given in fig. 9. It should be emphasized that this optimization is for a radiator of fixed length considerably less than that of an unconstrained and optimized radiator. This does not affect the choice of gap very much, but leads to a smaller number of foils than would be dictated by a freely optimized radiator, and correspondingly poorer

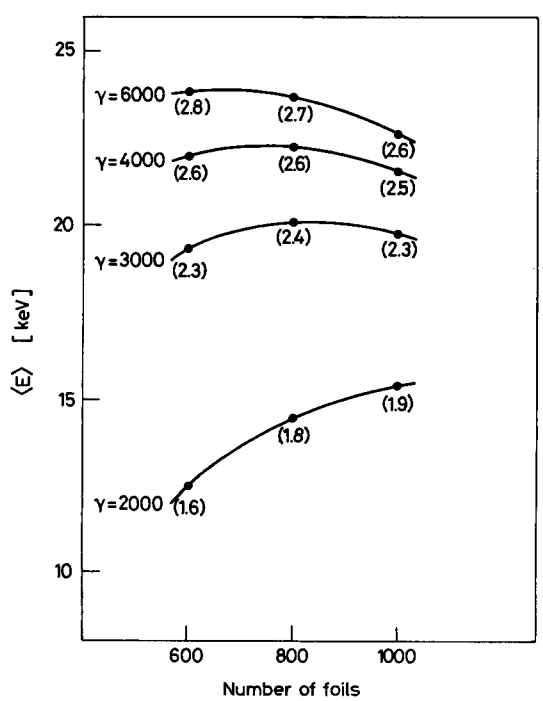

Fig. 9. Results of the optimization calculation for the 220 mm thick radiator using 50 μm thick Li foils. The numbers in brackets give the average number of photons emitted.

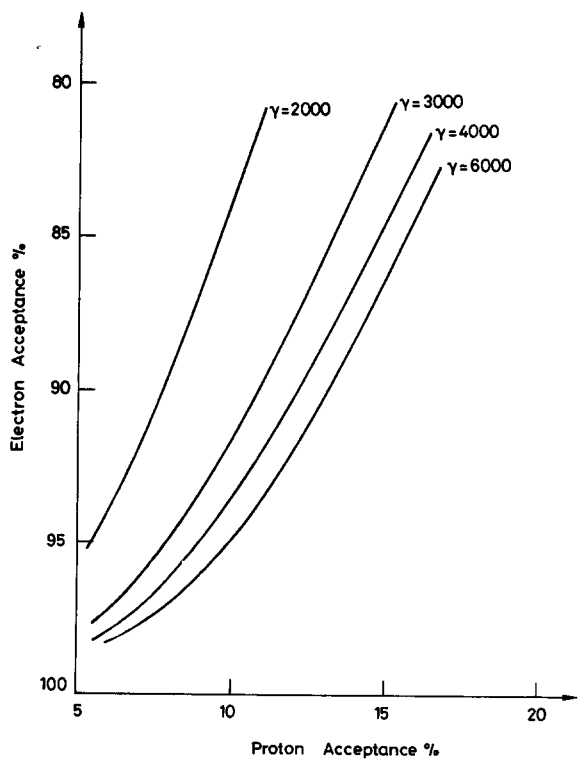

Fig. 10. Computed acceptance for electrons as a function of proton acceptance. A radiator of 220 mm thickness consisting of $N = 600$ foils, 50 μm thick, was assumed. The proton acceptance was measured for 12 GeV/c particles.

performance in particle identification. Furthermore, the thickness of the Li foils was chosen to be 50 μm, as thinner foils were considerably more difficult to handle. This choice resulted in a loss of about 13% of detected energy when compared to a radiator constructed with Li foils of optimum thickness, which was calculated to be ~ 35 μm. For this radiator we chose $N = 700$ foils, thus balancing TR losses for low γ with gains for higher γ-values. It also ensures a relatively large gap of 0.026 cm, which tends to minimize the effects due to fluctuations in the foil spacing. In fig. 10 we show for a $N = 600$ foil radiator the calculated detection efficiency for electrons of various momenta.

For the first series of measurements on these large radiators, the previously mentioned small test chamber was used. For this purpose a plexiglas plate was mounted on the exit face of the lithium box, with a 50 mm diameter mylar window in one position. In general, it is not satisfactory to use a mylar window to protect the lithium from the air because there is too much diffusion of water vapour through it, but it was adequate for the short duration of these tests.

The pulse-height distribution for electrons of 2 GeV/c is shown in fig. 11a; it is compared with the pulse-height distribution from 12 GeV/c protons in fig. 11b. The protons are somewhat above minimum owing to the relativistic rise in the xenon ionization loss. Fig. 11b also shows 2 GeV/c electrons, where 2 mm of aluminium have been introduced between the radiator and the chamber to absorb the X-rays. The electron ionization shows a strong relativistic rise. It is independent of energy in this region and is approximately 1.6 times the minimum ionization, while the protons are approximately 1.2 times the minimum ionization. The large amount of transition radiation in fig. 11a is very apparent, which is approximately six times the average energy loss of a minimum ionizing particle.

For the next series of measurements the lithium box was mounted directly on the large xenon MWPCs which are described in the companion paper[6]). Since this chamber and the small test chamber have the same depth and the same gas filling, the results should be the same. With the small chamber the property of the radiator was only measured in the vicinity of the thin window, but with the directly mounted proportional chamber, the entire surface of the radiator was scanned. The X-ray energy was found to be uniform to about 10%, except for the region immediately behind one of the steel blades that supports the window. The response was found to be uniform within less than 20 mm of the ends of the chamber.

A summary of the results is shown in fig. 12, where the average TR energy deposit in the MWPC is plotted as a function of momentum. The transition radiation is seen to rise very sharply above 0.7 GeV/c and to saturate quickly at about 2 GeV/c. This is a conse-

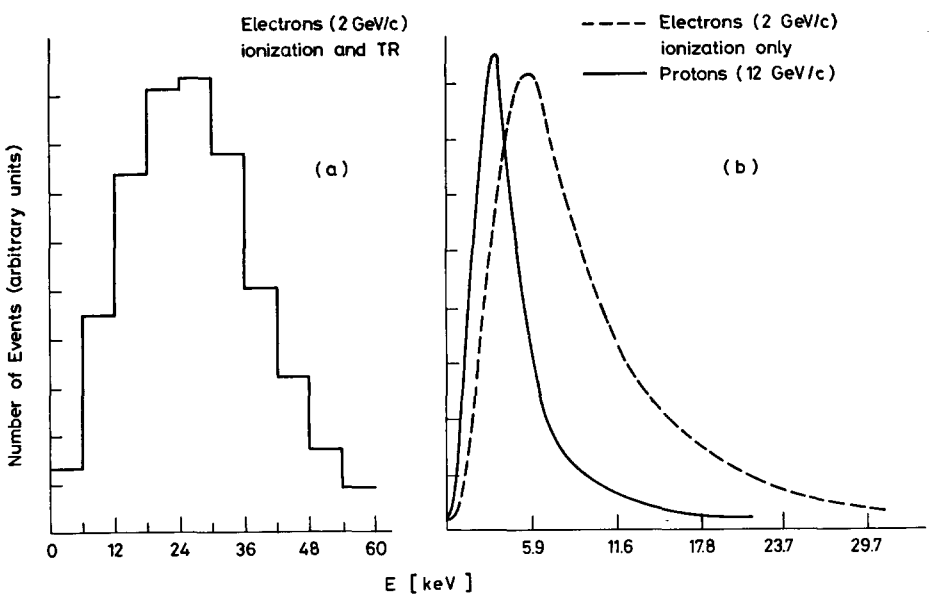

Fig. 11. (a) Measured TR yield for 2 GeV/c electrons measured with the small test chamber after a 56 mm air gap between radiator and chamber. (b) Measured ionization loss for 12 GeV/c protons and 2 GeV/c electrons. A 2 mm Al plate was placed between radiator and chamber to absorb the TR emitted by the electrons.

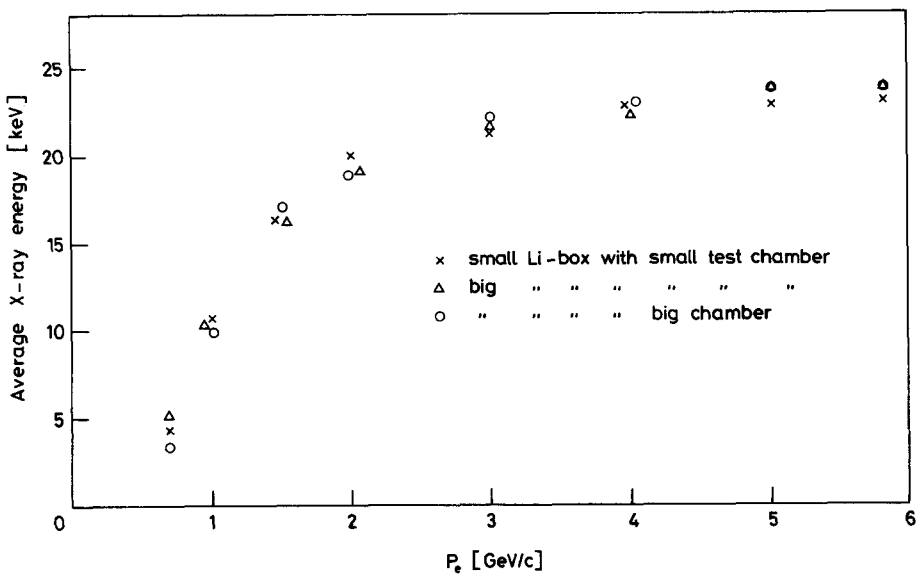

Fig. 12. TR yield as a function of electron momentum for several radiator-chamber combinations.

quence of the design of the radiator which has been chosen to place the constructive interference between all interfaces at an energy of approximately 1.5 GeV/c. The destructive interference shortly below this energy causes the rather sharp threshold, and similar effects give rise to the sudden appearance of the saturation at a somewhat higher energy. Our motivation for this

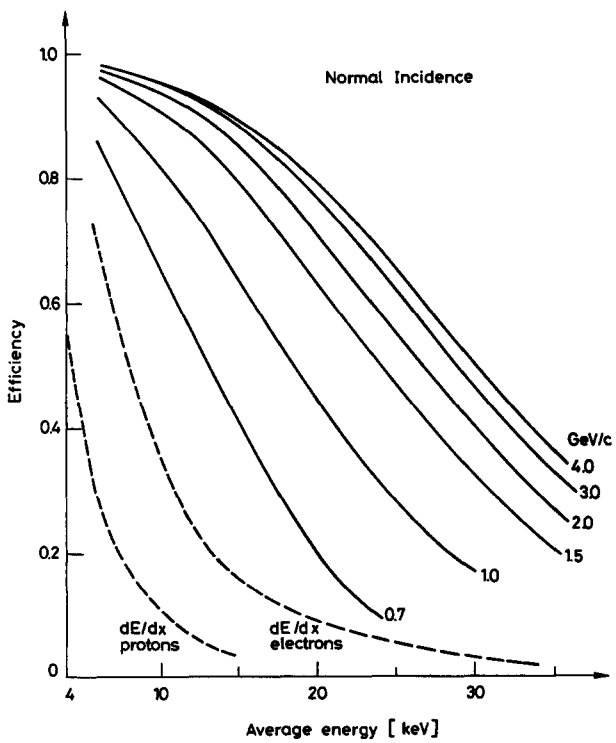

Fig. 13. The dependence of electron detection efficiency on energy threshold. For comparison, the integral ionization loss spectra for 2 GeV/c electrons and 12 GeV/c protons are also shown.

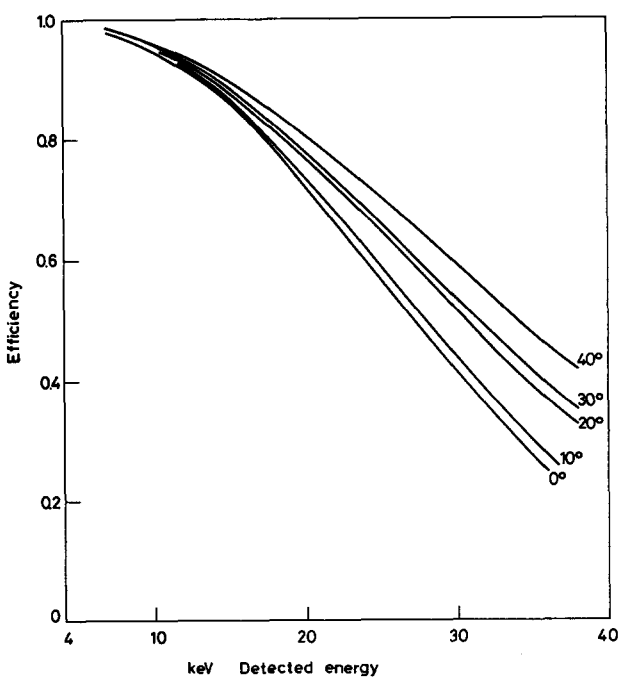

Fig. 14. Integral energy spectra for 2 GeV/c electrons for various angles of incidence. The angle is measured with respect to an axis normal to the chamber plane.

design was to produce the lowest practical threshold for detecting electrons, but the same properties would be especially valuable if it were desired to separate K mesons and π mesons at very high energies. The ionization of the electrons gives an additional $\langle E \rangle \simeq$ $\simeq$ 8 keV of energy which is not included in fig. 12, and which, owing to the relativistic rise, aids in the discrimination against particles of low γ. The equivalent data are plotted for two other radiator–chamber combinations. As neither the radiator nor the MWPCs were in principle different, identical results are expected and experimentally found.

These data are presented more conveniently for quantitative study as integral pulse-height spectra in fig. 13. Also included is the integral ionization loss spectrum for protons of $p = 12$ GeV/c and electrons of $p = 2$ GeV/c. As an example, we find that with an energy cut of 12 keV, 93% of 2 GeV/c electrons are accepted, while only 7% of the 12 GeV/c protons have an energy loss above this threshold.

When this assembly is rotated with respect to the beam, two compensating effects determine the performance of the detector. First, the energy deposited in the chamber by the ionization loss increases as sec θ. Second, the available path length for the absorption of X-rays is increased, so that there is some increase in the

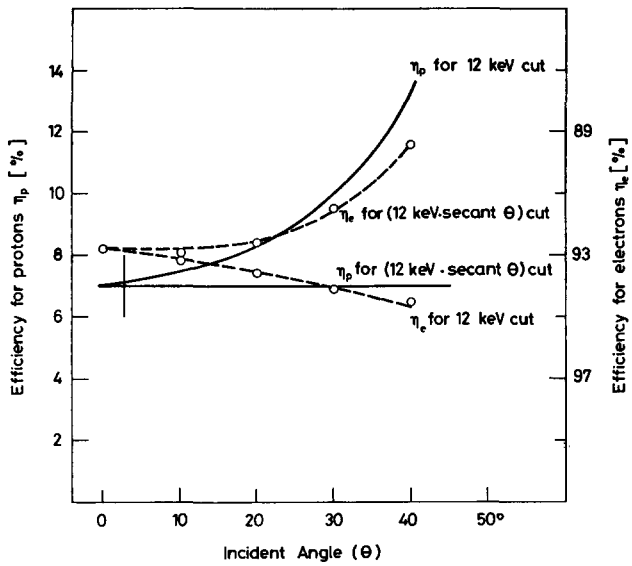

Fig. 15. Detection efficiency for protons (left scale) and electrons (right scale) for several angles of incidence. Data are given for 2 GeV/c electrons and plotted for a fixed 12 keV energy threshold and also for a threshold varying as 12 keV × sec. θ.

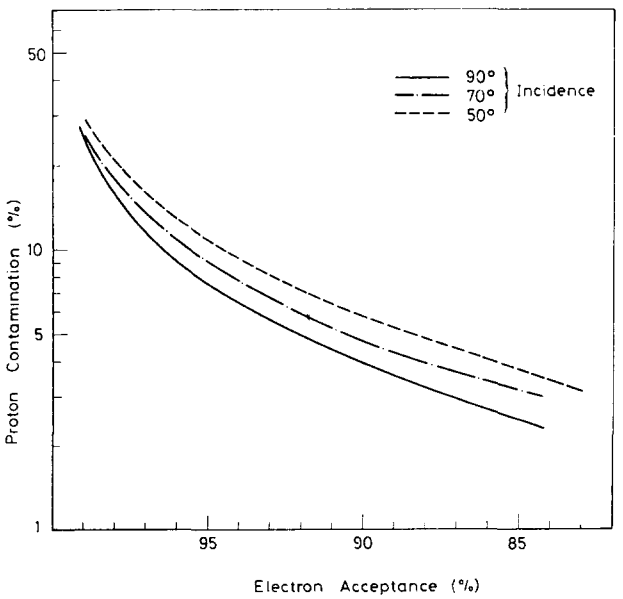

Fig. 16. Hadron contamination as a function of electron acceptance measured with *one* TRD of a TRD module. The angles of incidence are measured with respect to the plane of the Li foils.

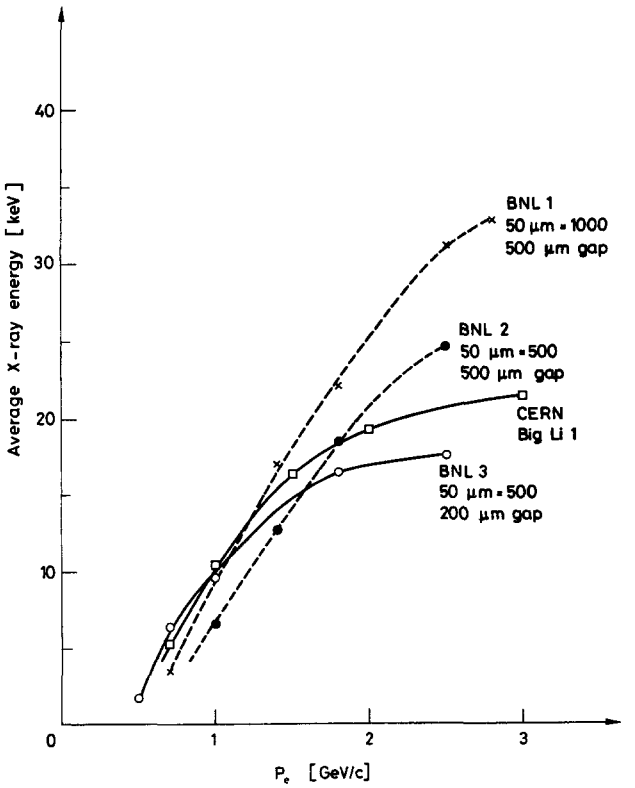

Fig. 17. Average TR energy measured from different radiators constructed from 50 μm thick Li foils. The number of foils and the gap spacing was varied. In all measurements a 12.7 mm thick MWPC was used, which was operated with an 80% Xe/20% CO_2 gas mixture.

amount of detected transition radiation. The net result is a tendency for the ratio of the transition radiation to the ionization loss to remain the same. Fig. 14 shows the integral pulse-height distribution as the angle with respect to the beam is varied. Fig. 15. shows the efficiencies for electrons and for minimum ionizing particles with a choice of accepted conditions: either a fixed cut of 12 keV, or a cut of 12 keV $\times \sec\theta$. It is seen that the properties in the detector can be maintained over a very wide angular range.

The integral pulse-height curves for different electron energies and angles can be used to construct curves showing the electron efficiency as a function of the hadron rejection. Fig. 16 shows three such curves. A substantial rejection factor can be achieved while maintaining a good efficiency. This is the first time that this has been achieved with a single radiator detector system. The use of the lithium radiator is the most important factor in this result, but the careful optimization of all parts of the detector is essential. Once a substantial rejection factor is achieved in one layer of detector, the rejection can be made very large by using a few layers. For the purposes of our experiment, two layers are sufficient. The effects of different choices of detector parameters are clearly exhibited in fig. 17, where the TR yield from various radiators is compared. In all cases a 12.7 mm thick MWPC, operated with a 80% Xe/20% CO_2 mixture, was used. It is particularly instructive to compare the two small BNL radiators, each consisting of 500 Li foils, 50 μm thick, but one with 200 μm and the other with 500 μm gap spacing. Because of interference effects, the latter radiator gives smaller TR yield at low γ's, but saturates at much higher γ-values ($\gamma_{sat} \simeq 8000$) with considerably increased TR emission.

5. Conclusions

We have shown that transition radiation detectors can be made which count electrons with good efficiency and achieve a substantial rejection of hadrons with a single detector. This detector does not degrade the particles, so that several layers can be used and still be followed by a shower counter for additional electron identification. The radiator is self-supporting so that it is practical to construct in large areas: up to now we have made more than 4 m^2. These detectors have been in use in an experiment in the ISR for about one year and have given a very satisfactory performance.

We should again emphasize that the design of such a detector must be carefully optimized since at best the number of transition radiation photons is just sufficient. If the requirements in another experiment were at all different from those in our own, the design of the radiator and detector might be appreciably different, but the method for optimization given in this paper should apply. For example, should the detector be used in a magnetic field, the deflection of the particle track away from the transition radiation should allow large rejection factors to be obtained in a single layer.

We are indebted to G. Muratori and K. Ley for assistance in the design and the construction of the dry room and the winding machine. We thank G. Dubois-Dauphin and K. Ley for their careful work in the fabrication of the radiators, and J. Fischer who provided the small proportional chamber for the tests.

References

1) V. L. Ginzburg and I. M. Frank, Z. Eksper. Teor. Fiz. **16** (1946) 15.
2) G. M. Garibian, Sov. Phys. JETP **10** (1960) 372; **33** (1971) 23; and Yerevan Report EØN-27 (1973).
3) A detailed review is given by M. L. Ter-Mikaelian, *High-energy electromagnetic processes in condensed media* (Wiley–Interscience, New York, 1972).
4) L. C. L. Yuan, in Proc. 5th Int. Conf. on *Instrumentation for high-energy physics*, Frascati, 1973 (CNEN, Frascati, 1973) p. 334.
5) J. Fischer, S. Iwata, V. Radeka, C. L. Wang and W. J. Willis, Phys. Lett. **49B** (1974) 393; Nucl. Instr. and Meth. **127** (1975) 525.
6) J. Fischer, J. Fuhrmann, S. Iwata, R. Palmer and V. Radeka, Nucl. Instr. and Meth., to be published.
7) X. Artru, G. B. Yodh and G. Menessier, Phys. Rev. D **12** (1975) 1289.
8) C. W. Fabjan and W. Struczinski, Phys. Lett. **57B** (1975) 484.
9) J. E. Bateman, Nucl. Instr. and Meth. **103** (1972) 565.
10) A. I. Alikhanian, in Proc. 5th Int. Conf. on *Instrumentation for high-energy physics*, Frascati, 1973 (CNEN, Frascati, 1973) p. 350.
11) P. Gorenstein and H. Gursky, Astrophys. J. **153** (1968) 885.